Fundamental Issues and Applications of
Shock-Wave and High-Strain-Rate Phenomena
K.P. Staudhammer, L.E. Murr, and M.A. Meyers (Editors)

Chapter 69

Self-organization of shear bands in stainless steel: grain size effects

Q. Xue, V. F. Nesterenko, and M. A. Meyers

Department of Mechanical and Aerospace Engineering
University of California, San Diego, La Jolla, CA 92093

Large assemblages (~200) of shear bands were investigated in stainless steel 304L through the radial collapse of a thick-walled cylinder under high-strain-rate deformation (~10^4 s^{-1}). This method was used to examine the shear-band initiation, propagation, as well as spatial distribution. Self-organization of multiple adiabatic shear bands was observed. Three grain sizes of the stainless steel were tested: 30, 50, and 140 μm. A single crystal of a similar composition was also tested. The effect of grain size on spacing of shear bands is discussed and no significant variation of the spacing was found in these steels. Three principal mechanisms are considered to be active in initiation: (a) momentum diffusion by stress unloading, (b) perturbation in the stress/strain/temperature fields, and (c) microstructural inhomogeneities. The observed shear-band spacing is compared with existing theories. A discontinuous growth mode for shear localization under periodic perturbation is proposed. Self-organized initiation and propagation modes are discussed in relation to the interaction among the nucleus and well-developed shear bands. The evolution of spacing of shear bands is associated with different growth stages, which are dictated by competitive mechanisms.

1. INTRODUCTION

Thermally-assisted shear localization, often called adiabatic shear band(SB), is one of the important failure mechanisms in materials deformed at high strain rates. The inhomogeneous plastic deformation leads to non-uniform distribution of heat, which promotes material softening and accelerates catastrophic failure. Adiabatic shear bands have been extensively studied[1] since the heat feedback mechanism was proposed by Zener and Hollomon[2]. Many efforts have been made to associate the metallurgical characteristics with the sensitivity to shear localization[3]. Multiple shear bands are often found in dynamic deformation, such as explosion and impact. The evolution of multiple shear bands exhibits some features of self-organization. The spatial distribution of shear bands has been shown experimentally to have a characteristic periodic spacing[4]. Grady[5], Grady and Kipp [6], Wright and Ockendon [7], and Molinari [8] gave theoretical predictions for shear band spacing that represent a beginning of our understanding of their collective behavior. However, there are very few reports that deal with the experimental determination of the spatial distribution of shear bands. Nesterenko et al. [9] developed an explosive testing method with thick-walled cylinder specimens, which was successfully used to investigate the spacing pattern of shear bands in stainless steel, titanium, and Ti-6Al-4V alloy [4, 9-11]. The dependence of shear band spacing on grain size in copper was reported in [12]. The purpose of this paper is to characterize the evolution of multiple shear bands in a typical f.c.c. material (stainless steel) and to analyze the spacing character. The effects of grain size and annealing on shear-band sensitivity, nucleation, and their spatial pattern are addressed. Two-dimensional effects among shear bands are considered in a simple evolving model for shear- band spacing.

2. EXPERIMENTAL PROCEDURE

The experimental configuration of the thick-walled cylinder explosion technique is described elsewhere[4,9]. The specimen was sandwiched between a copper driver tube and a copper stopper tube and was collapsed inwards during the test. The internal diameters of copper were selected to produce prescribed and controlled final strain. In some special cases a central steel rod was also used.

The maximum shear strain occurs on the internal surface of the cylindrical specimen, and thus shear bands preferentially initiate there. After each

experiment, the cylinders were sectioned and the lengths of shear bands, l_i, the edge displacements, δ_i, the average radius of final internal boundary, R_f, and the angle between spatial position from origin, Ψ_i, were measured as shown in Figure 1. In order to compare the deformation at the different positions on the specimen, an effective strain is used as [4]:

$$\varepsilon_{ef} = \frac{2}{\sqrt{3}}\varepsilon_{rr} = \frac{2}{\sqrt{3}}\ln\left(\frac{r_0}{r_f}\right) \quad (1)$$

where r_0, r_f are the initial and final radii of a reference point. The effective global strain at the internal boundary of the specimen is considered as a characteristic value of deformation since all the specimens have the same initial dimensions. Based on the number of distinguishable SBs, the average spacing between them is:

$$L = \frac{\Psi_i R_f}{n_i\sqrt{2}} \quad (2)$$

where n_i is the number of shear bands at the particular region i and Ψ_i is the corresponding angle for this region. If $n_i=n_{total}$, $\Psi_i=2\pi$. The spacing between shear bands decreases as plastic deformation proceeds. This effect was subtracted from the results with an appropriate correction. Thus, the spacings represent values at the initiation of the bands. The geometrical configuration contribution to the spacing variation was removed from the calculation of the shear band spacing by considering the smallest effective strain as the initial stage of shear localization. Hence, the spacing of shear bands can be expressed as:

$$L = \frac{\Psi_i R_f}{n_i\sqrt{2}}\left(\frac{R_{f0}}{R_f}\right) \cong \frac{\sum_i L_{i,i-1}}{n_i}\left(\frac{R_{f0}}{R_f}\right) \quad (3)$$

where R_{f0} is the radius of the specimen at shear band initiation, and R_f is the final radius, at any larger effective strain. $L_{i,i-1}$ is defined as the spacing between i-th and i-1-th shear bands in Figure 1. Since $R_f < R_{f0}$, the corrected spacing based on the final configuration has a lower value.

An austenitic stainless steel (SS) AISI 304L(T-304L) was selected to investigate the evolution of shear band spacing. The as-received SS304L bar, with a diameter of one inch, was solution treated. The microstructure is mainly the equiaxed austenite with average grain size of 30 μm. The heat

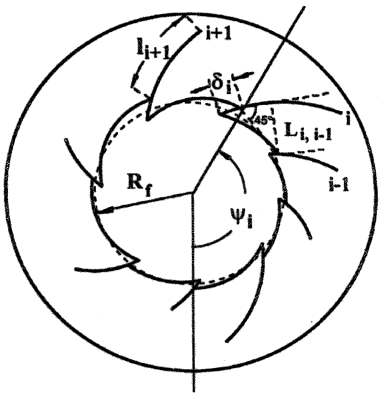

Figure 1. Characteristics of shear band pattern.

treatment conditions were selected to provide a wide variation of grain sizes: 800°C/3hr, 1050°C/3hr, and 1280 °C/3hr, followed by water quenching. The 800 °C/3hr annealed SS 304L has the same grain size as the as-received steel. The grain size of the steels annealed at 1050 °C/3hr and 1280°C/3hr are 50 μm and 140 μm, respectively. A single crystal of Fe-Ni-Cr alloy was also tested in the same configuration. The alloy content of 304L stainless steel is: Cr (18.37%) and Ni (8.18%), whereas the single crystal has a composition of Cr (15%) and Ni (15%). The total alloy content was approximately the same. Quasi-static and dynamic compression tests were carried out for materials under all different heat treatment conditions. The high-strain-rate mechanical response was measured by means of compressive split-Hopkinson bar experiments. Figure 2 shows the true stress-strain curves for both the as-received and 800°C annealed

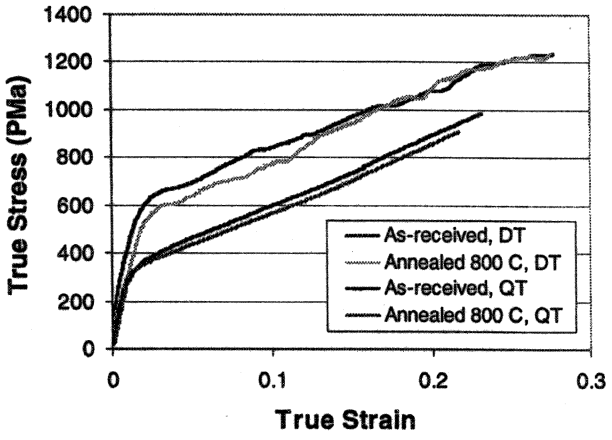

Figure 2. Compressive responses under quasi-static (QT, $\dot{\varepsilon}=10^{-3}$ sec^{-1}) and dynamic (DT, $\dot{\varepsilon}=10^{3}$ s^{-1}) conditions for the as-received and the annealed (800°C/3hr) stainless steel.

Table 1. Theoretical Predictions of Shear Band Spacing For Stainless Steel

	Grady-Kipp	Wright-Ockendon	Molinari (n=0, Without Strain Hardening)
Spacing	$2\pi\left[\frac{kC}{\dot{\gamma}^3 a^2 \tau_0}\right]^{1/4} \cdot \frac{9^{1/4}}{\pi}$	$2\pi\left[\frac{kC}{\dot{\gamma}^3 a^2 \tau_0}\right]^{1/4} \cdot m^{3/4}$	$2\pi\left[\frac{kC}{\dot{\gamma}^3 \tau_0 a^2}\right]^{1/4} \cdot \left[\frac{m^3(1-aT_0)^2}{(1+m)}\right]^{1/4}$
SS 304L	**2.62**	**0.17**	**0.16**

304L stainless steel bars. There is no significant difference between the two materials except for a little decrease in the strength for the annealed steel.

The thick-walled cylindrical specimen has the initial internal and external diameters as 14 mm and 21 mm, respectively. In the thick-walled cylinder explosion experiments, $\dot{\gamma}=6\text{x}10^4 s^{-1}$. The parameters for stainless steel are k=14.7 J/smK; C=500 J/kgK; $\tau_0=\sigma_0/2$ = 125 MPa. The strain rate sensitivity, m=0.012, was calculated from the quasi-static and dynamic tests; and the thermal softening factor is $a=7.2\text{x}10^{-4}$ K^{-1} from [13]. It can be seen from Fig.2 that the material work hardens substantially and that the Molinari theory is necessary to address this. The tensile properties listed by the manufacturer are: $\sigma_{0.2}$=250 MPa, σ_t =640 MPa, elongation Δ = 58%.

3. THEORETICAL PREDICTIONS

The current theories for predicting shear band spacing can be classified into two types. They start from the one-dimensional momentum and energy conservation equations, but are correlated with different mechanisms. One is based on the concept of momentum diffusion, and was developed by Grady and Kipp (GK) [6]. The basic idea lies in the unloading from the center of the SB and is inspired by Mott's [14] fracture work. The momentum diffusion due to the unloading creates a rigid region between the shear bands. The GK model uses a simple constitutive equation:

$$\tau = \tau_0 [1 - a(T - T_0)] \qquad (4)$$

There is no account for work hardening or strain rate effects. It is assumed that within a well-developed shear band the shear stress is reduced to zero; this corresponds to the later stages of shear localization with well developed shear bands.

The second approach uses the perturbation analysis at the critical transition from stable to unstable plastic deformation. Grady[5], and Wright and Ockendon (WO) [7] developed such an analysis for the one-dimensional simple shear case. The fastest growing perturbation wavelength associated with the instability corresponds to the minimum spacing in this approach. They selected a constitutive equation with strain-rate sensitivity and predicted the spacing of SBs. Molinari[8] modified the WO model by incorporating the effect of strain hardening into SB spacing. The WO constitutive equation is:

$$\tau = \tau_0 [1 - a(T - T_0)] \left(\frac{\dot{\gamma}}{\dot{\gamma}_0}\right)^m \qquad (5)$$

γ_0 is a reference strain rate and m is the strain-rate sensitivity. In order to compare these theories, we consider the predictions without strain hardening effect. The comparison of the three theoretical predictions for SB spacing is shown in Table 1. The GK, WO and Molinari models have a similar form, although they were developed from different assumptions. The only difference among them is in the coefficients, which describe the material parameters such as the strain rate hardening, m. The WO and Molinari models are the same except for a factor $[(1\text{-}aT_0)^2/(1+m)]^{1/4}$. Since m is much lower than 1, this factor is approximately $(1\text{-}aT_0)^{1/2}$. For $a=7.2\ \text{x}10^{-4}$, and T_0 =300K, the factor is 0.784. Thus, the Molinari and the WO predictions are of the same order. The GK model does not have a strain–rate sensitivity parameter and represents the state of affairs in the later stages of the evolution of shear localization, when shear stresses are unloaded due to thermal softening. The difference between the predictions of the GK model and WO/Molinari models is roughly a factor of 10 for normal metals. For the SS, the values are given in Table 1; for the Molinari model the effect of strain hardening was not included. The shear-band spacings are about 0.17 mm for the WO/M theories. On the other hand, the Grady prediction is 2.62 mm, more than 15 times the WO/M estimation.

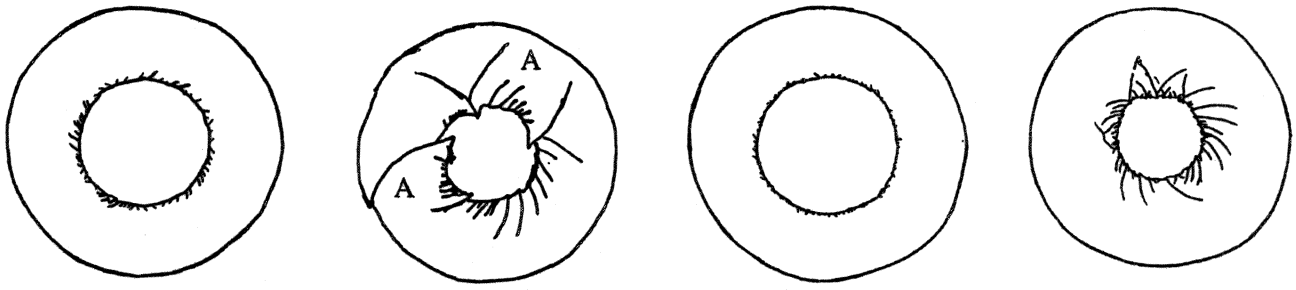

(a) As-received SS304L, ε_{ef} = 0.55, N=235 **(b) As-received SS304L, ε_{ef} = 0.92, N=165** **(c) Annealed SS304L, ε_{ef} = 0.55, N=186** **(d) Annealed SS304L, ε_{ef} = 0.92, N=194**

Figure 3. Evolution of shear band pattern in (a,b) as-received and (c,d) annealed stainless steels.

4. EXPERIMENTAL RESULTS

4.1 Effect of Annealing on Shear-Band Character

Two effective strains were applied: 0.55 and 0.92. Figures 3(a)~(d) show, in schematic fashion, the distribution of shear bands for the as received and annealed conditions. Only a small fraction of the bands are shown. The number of bands is marked in the bottom of each schematic. For as-received 304 stainless steel, the distinguishable number of shear bands is 235 at the effective strain ε_{ef}=0.55. At such a strain level these shear bands seems to develop in the initial stage. When the effective strain is increased to 0.92, the number of shear bands decrease to 165. For the annealed condition(800°C/3hr), the shear band number at ε_{ef}=0.55 is 186, while this number becomes 194 at ε_{ef}=0.92. There is a difference in the shear band pattern at larger effective strains. The longer shear bands block the development of the neighboring smaller shear bands. This is evidenced in Fig. 3(b) in the regions marked A. The longer bands forming an enclosure (because they are clock-wise and counter-clockwise), restrict the growth of the included bands. This phenomenon will be discussed further in Section 5.

A better quantitative assessment of shear-band evolution is provided by plotting shear band lengths L_i, as a function of position. Figure 4 gives the shear band distributions. At the initial stage (Fig.4(a) and (c)) the as-received steel exhibits more shear bands, and the length of shear bands is roughly four times that of the annealed steel. This indicates that the as-received steel has smaller critical strain for nucleation of shear bands and smaller spacing. At the well developed stage (Fig. 4(b) and (d)), the lengths of shear bands in the as-received steel are roughly double of the annealed. It is clear that the propagation velocities of shear bands in these two SS304 steels are different. If we assume that the propagating velocity for each material is a constant during the loading cycle(collapse of cylinder), the velocities of shear bands can be estimated. The thick-walled cylinder test provides a radial strain rate of about 3 x 10^4 1/sec[2]. The duration between the two effective strains is 8 μs. The increases of shear band lengths are 5.47 mm for the as-received steel and 2.68 for the annealed steel. This corresponds to propagation velocities of 684 m/s for the as-received steel and 335 m/s for the annealed steel.

The numbers of shear bands for the two 304 steels show the different tendencies. The number of shear bands in the as-received steel decrease with the increase of the effective strain, while the number in the annealed steel is almost constant, only slightly increased. It seems anomalous that the number of distinguishable shear bands at small effective strain is larger than that in large strain. The shear band pattern in the later stage shows that some initial shear bands disappeared and the surviving shear bands compose a new distribution. A fraction of these initial shear bands stop due to the unloading caused by the adjacent shear bands as the global strain is increased. The small shear bands submerged into the surrounding region at large deformation become undistinguishable in the heavily deformed material. The surviving shear bands were self-organized into a new spatial distribution with a characteristic spacing. This is discussed in Section 5.

The spatial distribution of shear bands depends upon both the available initial nucleation sites and

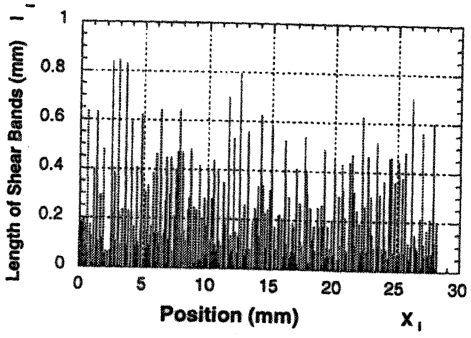

(a)As-received SS304 (ε_{ef}=0.55)

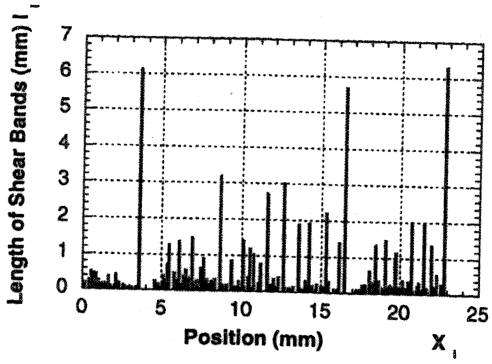

(b) As-received SS304(ε_{ef}=0.92)

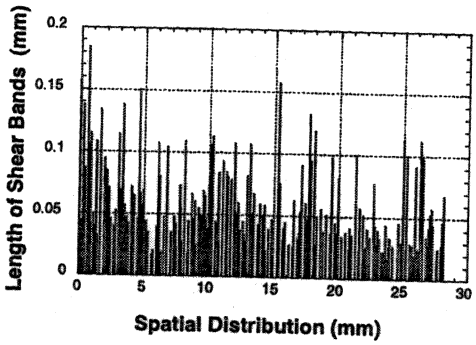

(c) Annealed SS304L Initial stage (ε_{ef} = 0.55)

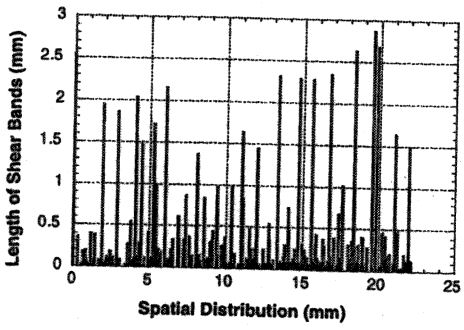

(d) Annealed SS304L Later stage (ε_{ef} = 0.92)

Figure 4. Shear band distribution in (a,b) as-received and (c,d) annealed 304 SS at different stages.

the interaction among the nuclei of shear bands. For the as-received condition, at an effective strain of 0.55, the spacing of shear bands is L_i=0.12 mm. At the well-developed stage, with ε_{ef}=0.92, the corresponding spacing becomes 0.16 mm. For the annealed condition the associated shear band spacings are 0.15 mm for ε_{ef}=0.55 and 0.15 mm for ε_{ef}=0.92, respectively.

The WO and Molinari perturbation models give a closer capacity of prediction (0.17 and 0.16 mm) to the experimental result, while the predicted spacing by GK model (2.62 mm) seems to be far from the experimental data. Although there is a difference of the spacings between the as-received and the annealed stainless steel, both of them are of the same order. A very important fact needs to be emphasized: there are several levels during the development of spacing pattern of shear bands. The WO/M models, based on perturbation analysis, reflect the behavior of shear bands at the initial plastic deformation stage. The GK model considers the extreme case in which the shear band totally loses its resist load. We need to consider a critical cut-length for the evolving shear bands. The application of the cut-off length of shear bands means that the shear bands with their length shorter than this value are "dead" and the only "living" shear bands can be considered to construct the new spatial pattern. For example, suppose that the critical length for our stainless steel is 0.18 mm; there are 11 shear bands in both the as-received and annealed SS304 from the spectrum of shear bands in Figure 4(b) and (d). The final "live" (i.e. propagating) shear bands construct a new spacing of 2.6 mm, which is fairly close to the GK prediction.

The difference of shear band spacings in the two kinds of stainless steels is directly related to the microstructure. Figure 5(a) and (b) show the configurations of shear bands at initial stage (ε_{ef}=0.55) for the as-received and annealed steels. It is clear that the edges of shear bands in the as-received steel are sharp at the internal boundary of the specimen (Figure 5(a)), which is locally straight. The shear bands, once nucleated, immediately propagate into the depth of the cylinder specimen at the angle 45° to the radius. Each shear band unloads the surrounding area and make adjacent parts slide out of the surface. The length of the edge is 62.5 μm and the corresponding width of shear bands is about 10 μm. The local shear strain at the root of the edges shear band reaches more than 6. However, under the

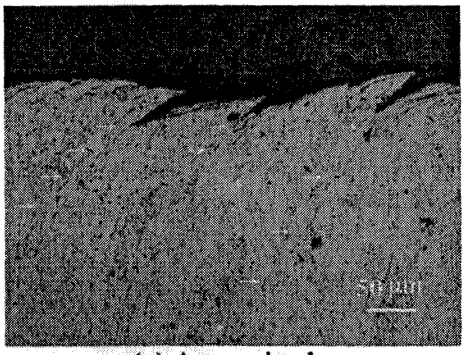

(a) As-received

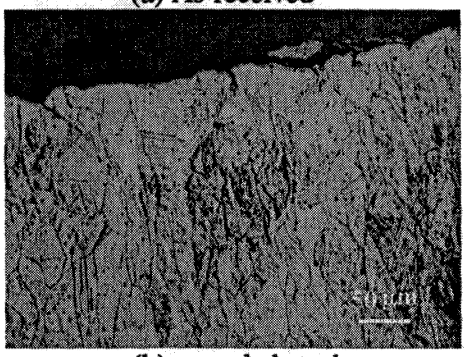

(b) annealed steel

Figure 5. The configurations of shear bands at initial stage $\varepsilon = 0.55$ (a)as-received steel (b) annealed steel.

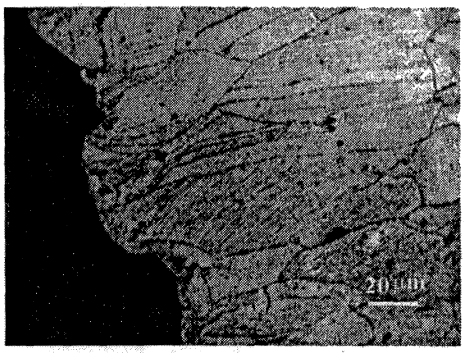

Figure 6. Wavy surface without shear band initiation in the annealed 304 steel.

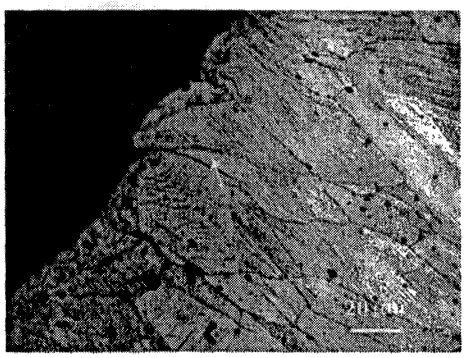

Figure 7 Short shear band blocked by a grain boundary in the annealed steel(see arrow).

same effective strain, the annealed steel reveals to be hard to produce a localized shear deformation and follow the path of largest shear stress. Figure 5(b) shows that the edges of the sliding parts at the internal surface were blunted with the characteristic size of hump covered a few grains. It is clear that large grain size in the annealed steel is able to block the nucleation of shear bands through localization of deformation within individual grain.

The close-up observation for the annealed steel reveals two main barriers to retard propagation of localized deformation. One of them is the slow squeeze-out of the grains, caused by easy slip systems in individual grains. In Figure 6, there is no localized deformation although some of grains were squeezed out to form a wavy surface. The wavy boundary may provide further nucleation sites of shear bands, but it absorbs a large deformation energy and blocks the development of the localized deformation. The other is a grain boundary effect. Figure 7 shows that a shear band was blocked within one grain. Although the local shear strain is equal to 3.2, the shear band cannot propagate through the grain boundary. Instead, it branches into several small shear bands and is dispersed in this grain. The annealing of steel significantly reduces the density of dislocations within the grains. It leads to the softening of material. The low density of dislocations of crystal grains in the annealed steel is considered to response to this behavior. However, machining of the surface could have predisposed the as-received SS to shear localization, whereas the specimen in the annealed condition was pre-drilled. A highly work hardened surface layer could have affected the results. A separate experiment is planned to verify this effect.

4.2 Grain Size Effects on Shear Band Character

The stainless steels annealed at 1050°C and 1280°C show different grain sizes from the as-received steel. The spatial distributions of shear bands in these two annealed steel are shown in Figure 8(a) and (b). The spacings of shear bands are 0.15 mm for the 1050°C annealed steel and 0.16 mm for the 1280°C annealed steel, respectively. Comparing with the spacing of 0.15 mm for the 800°C annealed steel, the spacings of shear bands seem to be kept as the same value. This result shows that no grain size effects on the spatial distribution of shear bands. The above result is also estimated from the current theories. WO model suggested that the

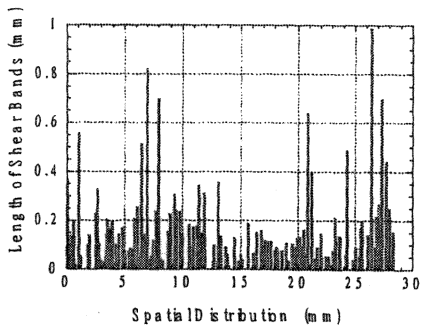

(a)Annealed 1050°C

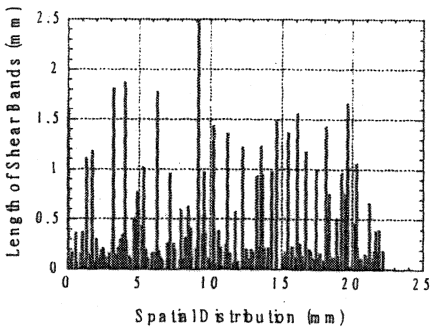

(b) Annealed 1280 °C

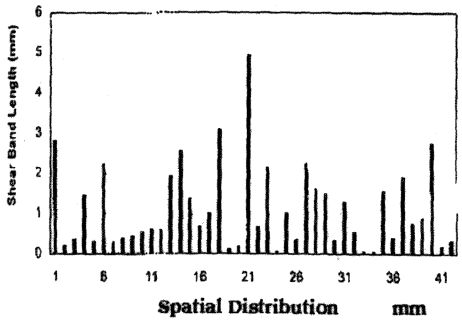

(c) Single crystal of Fe-Cr-Ni alloy

Figure 8. The Spectrum of shear bands (a) annealed steel, d=50 μm, ε = 0.55, n=190 and (b) annealed steel, d = 140μm, ε = 0.92, n=184. (c)single crystal of Fe-Ni-Cr alloy, n = 42.

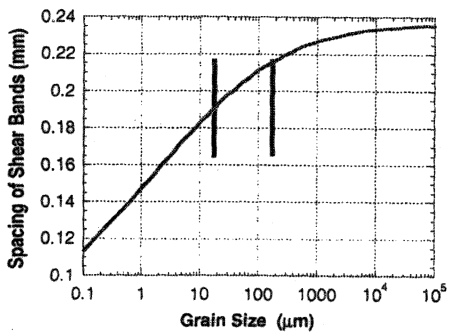

Figure 9. Relation between shear band spacing and grain size (WO theory).

shear band spacing is determined by several parameters of the tested material:

$$L_{wo} = 2\pi\left(\frac{m^3 kC}{\dot{\gamma}_0^3 a^2 \tau_0}\right)^{1/4} \qquad (6)$$

where τ_0 is the flow shear stress at the reference temperature T_0 and strain rate $\dot{\gamma}_0$. The relation between the flow stress and the grain size is obtained from the Hall-Petch equation:

$$\tau_0 = \tau_{01} + k_1 d^{-1/2}. \qquad (7)$$

If Tresca's flow rule is considered in this case, the shear flow stress is half of the normal flow stress. The parameter k_1 for 304 stainless steel is 0.35 $MNm^{-3/2}$ from [15]; τ_{01} is 61.1 MPa. Using Equations (6) and (7), the spacing variation with grain size is expressed as:

$$L_{wo} = 2\pi\left(\frac{m^3 kC}{\dot{\gamma}_0^3 a^2 (\tau_{01} + k_1 d^{-1/2})}\right)^{1/4} \qquad (8)$$

The single crystal alloy Fe-15Cr-15Ni has a composition similar to 304L steel(18Cr-8Ni). Its quasistatic yield stress is approximately 70 MPa. The shear-band pattern, shown in Figure 8(c), indicates that the number of shear bands is significantly lower for the single crystal. This is in full agreement with Eqn.(8). Indeed, the yield stress is lower than that of 304L SS: 125 MPa. Figure 9 shows the dependence of the spacing on grain size according to Eqn. (8). Since the flow stress effect has the power of ¼, the spacing is not greatly affected. The range of grain sizes that our experimental data covers is also marked in the Figure 9. This estimation is in rough agreement with the experimental results. It is concluded that there is no significant effect of grain size on the shear band spacing for the range of grain sizes studied(30-140 μm).

5. EVOLUTION OF SHEAR BAND SPACING: TWO-DIMENSIONAL EFFECTS

It is clear that collective organization processes take place during the formation of shear bands. It is also clear that two-dimensional effects, not incorporated into the GK or WOM theories, are important. These two-dimensional effects need to be considered and a preliminary attempt is made here. The description of the evolving process of the shear band patterns is much complicated not only because the development of a single shear band depends on multiple material parameters but also because the interaction among shear bands dominates the

evolution of their pattern. All current theories are based on the analysis of a single shear band. The influence of interaction of shear bands on its evolution has never been considered. Therefore, they, in some extent, can not explain the self-organization behavior of shear band pattern. Three important factors determine the development of shear-band spacing: the rate of nucleation, the rate of growth (or the velocity of shear bands), and characteristic time of interaction between shear bands.

(a) Initiation stage:

Shear bands arbitrarily nucleate at the internal boundary of the specimen, at sites determined by the small perturbations of initial deformation, at favorably oriented grains and defects. However, there is a continuing shielding effect, so that the bands that actually grow are often a small fraction of the total possible initiation sites. We will first describe the nucleation of bands with increasing plastic strain, ε.

The probability of nucleation, $P(V_0)$, in a reference volume, V_0, can be described by a modified Weibull distribution, using strain as the independent variable (in lieu of stress, in the conventional approach). Thus, it is equal to:

$$P(V_0) = 1 - \exp\left[-\left(\frac{\varepsilon - \varepsilon_i}{\varepsilon_0 - \varepsilon_i}\right)^q\right], \qquad (9)$$

where ε_i, is the critical strain below which no initiation takes place; ε_0 is the average nucleation strain(material constant); ε is the variable; and q is a Weibull modulus. The relation between $P(V_0)$ and ε is given in Figure 10. The critical strain and the mean nucleation strain are selected as 0.3 and 0.5, respectively, to best fit the experimental results for stainless steel; q was given values of 3, 5, 7, and 9, providing different distributions. The different Weibull moduli reflect the dispersion of shear band nucleation. For different materials the nucleation curve can have different shape and position, adjusted by setting q, ε_i, and ε_0. The rate of nucleation can be obtained by taking the time derivative of the above expression. In the geometry used in the experiments, V_0 can be replaced by a distance, L.

Figure 11 shows the schematic interaction between embryos, and growing shear bands. Each growing band generates a shielded region around itself, that is the result of unloading. We assume, to a first approximation, that the width of the unloaded region is twice the length of the shear band[16]. Indeed, this is approximately observed in our experiments. The distributions in Figure 4 indicate that the length of the shear bands is approximately equal to the spacing at the higher strains. Three factors govern the evolution of self organization: (a) the strain rate, $\dot{\varepsilon}$; (b) the velocity of growth of shear band, V; (c) the initial spacing, L. Figure 12 shows three possible outcomes, dependent on the growth velocity V. The activation of embryos is shown at three times, t_1, t_2, and t_3. When V is low, the embryos are all activated before shielding occurs, and the natural spacing L establishes itself. As V increases, shielding becomes more and more important, and the number of disactivated embryos increases.

This shielding effect can be expressed as:

$$S = \frac{k_0 V}{\dot{\varepsilon} L} \qquad (10)$$

This expression correctly predicts an increase in shielding S with increasing V, decreasing $\dot{\varepsilon}$, and decreasing L. The value of the parameter k_0 can be obtained by setting the total strain range for nucleation as $2(\varepsilon_0-\varepsilon_i)$:

$$k_0 = 2 \cdot (\varepsilon_0 - \varepsilon_i) \qquad (11)$$

The probability of nucleation under shear band shielding becomes P(L):

$$P(L) = (1 - S) \cdot P(V_o) = \left(1 - \frac{2(\varepsilon_0 - \varepsilon_i)v}{\dot{\varepsilon} L}\right)\left\{1 - \exp\left[-\left(\frac{\varepsilon - \varepsilon_i}{\varepsilon_0 - \varepsilon_i}\right)^q\right]\right\} \qquad (12)$$

Figure 12 shows predicted evolutions of nucleation probabilities as a function of increasing strain, for

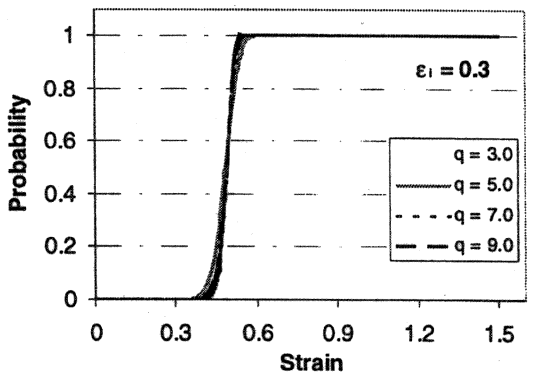

Figure 10. The probability of nucleation of shear bands as a function of shear strain for four values of q: 3, 5, 7, and 9.

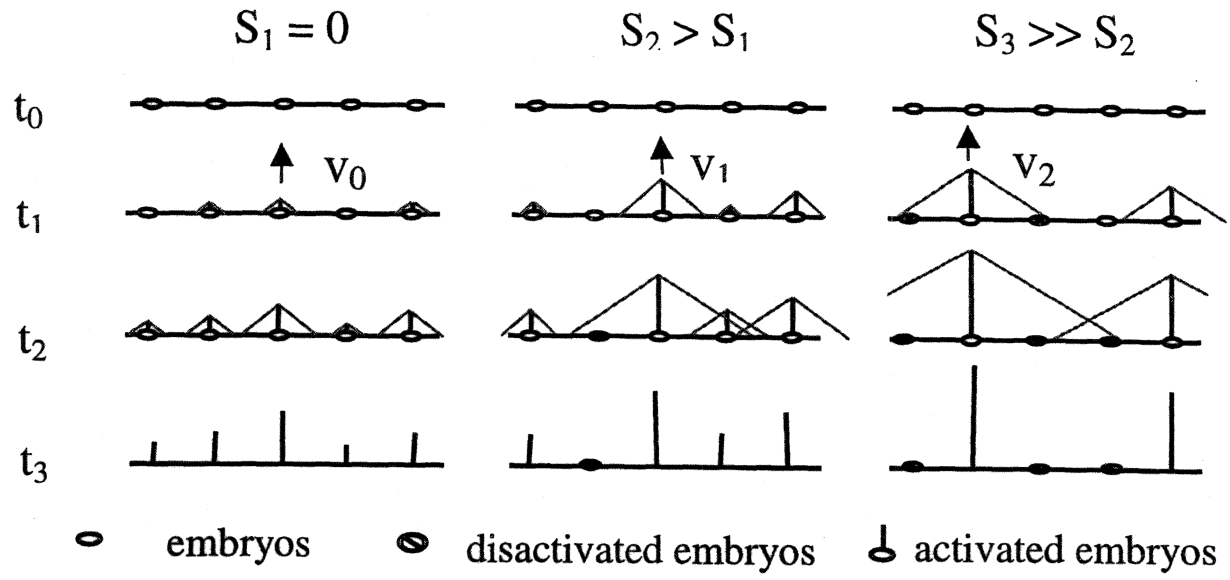

Figure 11. Two-dimensional representation of nucleation and shielding.

different values of the shielding factor, S: 0.0, 0.2, 0.4, 0.6. This simple model has the correct physics and shows how the initial distribution of activated embryos can be affected by different parameters.

(b) Growth stage:

Once the shear bands grow to a certain dimension, they meet some barriers such as grain boundaries and slow down. They seem to wait for other small shear bands initiate and grow up to form an approximately periodical pattern. In this stage shear bands pattern shows a self-organization phenomenon.

The further deformation makes the heterogeneous growth of these shear bands. Some shear bands grow faster than the others. The unloading of the fast-developed shear bands reduces the speed of the

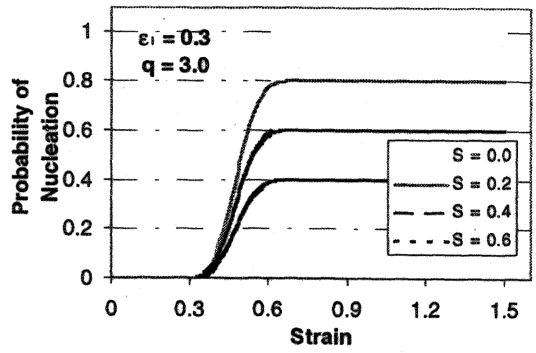

Figure 12. Effect of shielding on the probability of nucleation as a function of plastic strain.

adjacent small shear bands, and creates the heterogeneous growth (see SBs in Figure 3(b)). The favorable shear bands grow faster, while the unloaded shear bands slow down, and finally stop. The "living" shear bands compete each other and construct a new spatial pattern by following the self-organization rule. The dead small shear bands may leave at their original location, or may be merged into the large plastic deformation of the surround area. In this case the number of shear bands effectively reduces as it happened in the later stage of the as-received stainless steel specimen.

The dominant factors in this process depend on the material parameters, constitutive character, loading condition, and strain rate.

The velocity of shear bands, relative to unloading, is an important factor that affects their spatial distribution, an aspect which the current theories have not covered. In the extreme case when time of propagation of shear band through specimen is smaller than the characteristic time of shear band interactions, no self-organization will take place. The driving force for shear-band propagation is the elastic energy release. The rate of initiation is quite different from the growth rate (or growth velocity). It is reasonable to suggest that the growth is governed by stress, whereas initiation is governed by strain. The necessary condition is:

$$\tau_g < \tau_i, \qquad (13)$$

where τ_g and τ_i are the critical shear stresses for growth and initiation, respectively. The greater the difference, the higher the velocity of propagation. The unloading waves sweep through the surrounding area of a shear band and make new nucleation within this area impossible.

The interaction of shear bands leads to the competitive growth of the propagating shear bands. In previous theories the interaction among shear bands can only be treated as one-dimensional event at the simplest, elementary level. The volume of material shielded from further nucleation and growth increases with the length of a shear band in cylindrical geometry and is not constant, as predicted with these elements in place, one can construct a more realistic two-dimensional theory for the evolution of the self-organization of shear bands.

This phenomenon is analogous to the increasing spacing of propagating parallel cracks studied by Nemat-Nasser et al. [17]. Different evolution stages for shear bands are schematically indicated in Figure 13. At a certain length l_i, the spacing is L_i; the

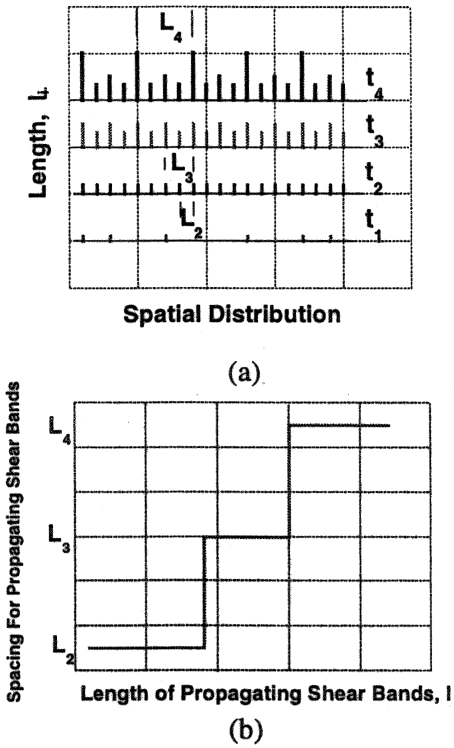

Figure 13. (a) Schematic diagram of the evolution of shear band spacing at different levels: t_1-random initiation; t_2-self organization into "periodic" pattern among nuclei; t_3-some shear bands grow faster suppressing others; t_4-self organization of developed shear bands, (b) spacing of propagating shear bands as a function of length.

growth becomes unstable at a critical length $l_{cr,i}$, and alternate SBs grow with a new spacing L_{i+1}; the other shear bands stop growing. The mathematical representation of the step function shown in Fig.14b is

$$L = L_0 + \sum_{j=1}^{n} k_j' \cdot H\left(l - l_{cr,j}\right) \qquad (14)$$

where $H(l-l_{cr,i})$ is a Heaviside function. The parameters k_j' can be expressed as:

$$k_j' = f(v, L_0, \varepsilon_i, \varepsilon_p), \qquad (15)$$

where v is the shear band propagation velocity, L_0 is the initial spacing, ε_i, is the critical strain for initiation and ε_p is the critical strain for propagation.

6. CONCLUSIONS

Shear band characteristics and spacings in stainless steel 304L were experimentally investigated. The effects of material parameters on the initiation and spatial distribution of shear bands are analyzed. The spacings of "living" shear bands are shown to evolve during the deformation process. Comparison with analytical predictions shows that the WO/M model predicts the initial level of self organization of shear bands, while the GK model shows a better agreement with the behavior at the developed stage of shear bands. The as-received 304 steel shows higher sensitivity to initiation of shear bands and the catastrophic development of few of them in comparison with the annealed one. The softening and the low density of dislocations of crystal grains in the annealed steel are considered to be responsible for this behavior. The grain size exerts some effect on the spacing of shear bands, but no significant change occurs in the range of the tested grain sizes. The current theories do not include the effects of shear band interaction and growth velocity. A discontinuous growth mode is proposed, wherein the spacing changes periodically, when the spacing reaches the interaction distance between adjacent shear bands, which is a function of their lengths. The self-organized initiation and propagation modes are discussed in a preliminary fashion from growth of some favorable shear bands.

ACKNOWLEDGMENT

This work was supported by U.S.A. Army Research Office under MURI program No. DAAH004-96-1-0376 (Program Manager David

Stepp). Discussions with and support by Dr. T. W. Wright are greatly appreciated. Prof. V. Lubarda's and Dr. D. Curran's help are gratefully acknowledged.

REFERENCES

1. Y. Bai, and B. Dodd, Adiabatic Shear Localization, Pergamon, Oxford, 1992.
2. C. Zener and J.H. Hollomon, J. Appl. Phys., 15 (1944) 22.
3. H.C. Rogers, Ann. Rev. Mat. Sci., 9 (1979) 283.
4. V.F. Nesterenko, M.A. Meyers, and T.W. Wright, Acta Mat., 46 (1998) 327.
5. D. Grady, J. Geoph. Res., 85 (1980) 913.
6. D.E. Grady and M.E. Kipp, J. Mech. Phys. Solids, 35 (1987) 95.
7. T.W. Wright and H. Ockendon, Int. Journal of Plasticity, 12 (1996) 927.
8. A. Molinari, J. Mech. Phys. Solids, 45 (1997) 1551.
9. V.F. Nesterenko, A.N. Lazaridi, and S.A. Pershin, Fizika Goreniya i Vzryva, 25 (1989) 154.
10. V.F. Nesterenko and M.P. Bondar, DYMAT Journal, 1 (1994) 245.
11. Q. Xue, V.F. Nesterenko, and M.A. Meyers, in"Shock Compression of Condensed Matter-1999", AIP Conf. Proc. 505, ed. M.D. Furnish et al., AIP Press, New York, (1999) 431.
12. V.F. Nesterenko, M.P. Bondar', and I.V. Ershov, "High-Pressure Science and Technology-1993", ed. by S.C. Schmidt et al., AIP Conf. Proc. 309, AIP Press, New York , (1993) 1173.
13. M.G. Stout and P.S. Follansbee, Trans. ASME., J of Eng Mat. & Tech, 108(1986) 344.
14. N. F. Mott, Proc. Roy. Soc., 189 (1947) 300.
15. H.-J. Kestenbach and M.A. Meyers, Metall. Trans. A, 7A (1976) 1943.
16. D.R. Curran and L. Seaman, in "Shock Waves in Condensed Matter", ed. Y.M. Gupta, Proc. of The Fourth APS Topical Conf., Plenum, New York, (1985) 315.
17. S. Nemat-Nasser, L.M. Keer, and K.S. Parihar, Int. J. Solids Structures, 14 (1978) 409.